

Understanding Adversarial Robustness from Feature Maps of Convolutional Layers

Cong Xu , Min Yang 

Abstract—The adversarial robustness of a neural network mainly relies on two factors, one is the feature representation capacity of the network, and the other is its resistance ability to perturbations. In this paper, we study the anti-perturbation ability of the network from the feature maps of convolutional layers. Our theoretical analysis discovers that larger convolutional features before average pooling can contribute to better resistance to perturbations, but the conclusion is not true for max pooling. Based on the theoretical findings, we present two feasible ways to improve the robustness of existing neural networks. The proposed approaches are very simple and only require upsampling the inputs or modifying the stride configuration of convolution operators. We test our approaches on several benchmark neural network architectures, including AlexNet, VGG16, RestNet18 and PreActResNet18, and achieve non-trivial improvements on both natural accuracy and robustness under various attacks. Our study brings new insights into the design of robust neural networks. The code is available at <https://github.com/MTandHJ/rmc>.

Index Terms—adversarial robustness, anti-perturbation ability, convolutional layer, feature maps, pooling

I. INTRODUCTION

ALTHOUGH deep neural networks (DNNs) have achieved compelling performance on many challenging learning tasks, some works [9], [31] found that they are vulnerable to artificially crafted adversarial perturbations. Imposing human imperceptible perturbations on clean samples could deceive the networks and cause incorrect classification. As a result, the vulnerability of DNNs impedes their deployment, especially in security-critical applications.

In order to evaluate the robustness of networks, a series of attack methods [3], [5], [9], [20], [21] have emerged. There is a consensus among them that, standardly trained DNNs have little robustness within human-imperceptible perturbation budgets. To mitigate this problem, numerous parallel defense methods [4], [9], [16], [34], [35], [39] have been developed to improve the robustness of DNNs, among which adversarial training [20], [38] is one of the most successful. Adversarial training enforces DNNs to correctly classify not only clean samples, but also their artificially perturbed counterparts.

We argue that the robustness of a neural network mainly relies on two factors, one is the feature representation capacity of the network, and the other is its resistance to perturbations. Usually larger neural networks tend to have better feature

This work is partially supported by National Natural Science Foundation of China under grant 11771257. (Corresponding author: Min Yang.)

Cong Xu and Min Yang are with the School of Mathematics and Information Sciences, Yantai University, Yantai 264005, China (email: congxueric@gmail.com; yang@ytu.edu.cn)

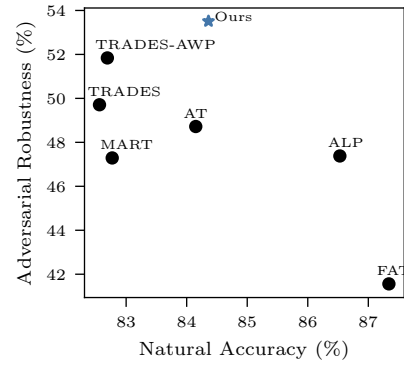


Fig. 1. Natural accuracy (%) and adversarial robustness (%) of ResNet18 on CIFAR-10 using different defensive models. Blue star indicates the result on our modified architecture trained with TRADES-AWP [35].

representation capabilities [2], [12], [30], which is why most robust results are based on large network architectures [11], [20], [36]. However, a larger network does not necessarily mean a better anti-perturbation ability. On the contrary, a larger network is likely to have a larger Lipschitz constant, which in turn leads to lower resistance to perturbations [14], [36]. Noticeably, a peculiar phenomenon often observed in adversarial robustness literature is that when the natural accuracy of a deep learning model increases, the corresponding robustness decreases, which also indicates that the anti-perturbation ability of the network is not consistent with its feature representation capacity.

As an important part of most DNNs, the structure of convolutional layer has a key influence on the final performance of the network. This paper aims to analyze the anti-perturbation ability of the network from the perspective of convolutional feature maps. We mainly focus on the dimensionality of the convolutional features. Our theoretical analysis reveals that larger convolutional features before average pooling can indeed contribute to better resistance to perturbations, but the conclusion is not true for max pooling. Experimental results also verify the above theoretical findings.

Based on the theoretical results, we propose two feasible ways to alter the convolutional architectures to enhance the robustness of neural networks. One approach is upsampling the inputs only, and the other is simply modifying the sliding stride configuration of convolutional operators. With the proposed methods, we achieve superior robustness improvements for benchmark neural architectures such as AlexNet [18], VGG16 [30], RestNet18 [12] and PreActResNet18 [13] using various defensive models, including AT [20], ALP [16], TRADES

[38], MART [33], FAT [39] and AWP [35]. Moreover, besides robustness, we also observe a surprising enhancement of natural classification accuracy on the modified network architectures. Therefore, the proposed methods not only help to strengthen the anti-perturbation ability of neural networks, but can also boost their feature representation capacity. We believe that the study of the paper will lead to a new perspective to understand the adversarial robustness of neural networks.

Our major contributions can be summarized as follows:

- We theoretically reveal that the anti-perturbation ability of neural networks is closely related to the feature maps of convolutional layers. Properly enlarging the dimensions of convolutional features before average pooling can improve robustness, whereas the opposite holds true for max pooling.
- Two effective ways with slight modifications on convolutional layers are presented to enhance the robustness of neural networks. Significant improvements are obtained for existing neural network architectures on both robustness and natural accuracy.
- The research expands the understanding of the robustness of neural networks, and brings in new insights for developing robust deep learning models.

II. RELATED WORKS

A. Robust learning strategies

Numerous robust learning algorithms have been developed from different perspectives to help neural networks achieve robust feature representations. For example, Cohen et al. [4] and Salman et al. [28] studied randomized smoothing technique that could transform any base classifier into a new smoothed classifier that is certifiably robust. Pang et al. [22] exploited the Max-Mahalanobis center loss to force the network to learn compact features. Adversarial training [20] is the most successful robust learning technique, which constructs the min-max optimization objective to dynamically fit the underlying distribution of adversarial samples. Among them, TRADES [38] and MART [33] contribute to a good trade-off between natural accuracy and robustness. FAT [39] minimized the loss over friendly adversarial samples, thereby enjoying superior natural accuracy. Nevertheless, adversarial training is known to suffer from over-fitting [25]. Therefore, an early-stopping learning schedule [11], [23] is preferred. In addition, some practical techniques such as adversarial weight perturbation (AWP) [35] and weight averaging [11] can help circumvent the local optima.

However, with the development of robust feature learning methods, the progress that can be made becomes more and more limited. It is imperative to study adversarial robustness from the perspective of neural network architecture.

B. Robust network architectures

The robustness of a neural network mainly relies on two factors, one is the feature representation capacity of the network, and the other is its resistance to perturbations. Naturally, one of promising directions is to promote the representation

capacity by using certain large networks. Unfortunately, deeper or wider networks are likely to have larger Lipschitz constants, which leads to lower resistance to perturbations [14], [36]. Therefore, it is of particular value to improve the robustness of the network from the perspective of anti-perturbation.

Recently, Dai et al. [6] studied the learnable parametric activation functions and the developed PSSiLU can significantly increase robustness when extra training samples are available. Shao et al. [29] showed that vanilla ViTs [7] can learn more generalizable features and thus has superior robustness against adversarial perturbations. It is also found in [14] that reducing capacity at the last stage of WideResNet [37] can enhance the adversarial robustness.

Although the above studies have made impressive robustness improvements in exploring network architectures, the research on designing robust network architectures is far from enough. Different from the perspective of existing studies, this paper investigates the anti-perturbation ability of neural networks from the feature maps of convolutional layers.

III. ANTI-PERTURBATION ABILITY OF CONVOLUTIONAL FEATURES

A. Preliminaries

A neural network $f(\cdot)$ is robust around a clean sample x with the label y , if the following two conditions are satisfied. First, identify the sample correctly, i.e.,

$$f(x) = y. \quad (\text{III.1})$$

Second, predict its perturbed counterparts consistently within a given perturbation budget ϵ , i.e.,

$$f(x + \delta) = f(x), \quad \forall \|\delta\|_\infty \leq \epsilon. \quad (\text{III.2})$$

For the entire dataset, the proportion of correctly identified clean samples is exactly the natural accuracy, which reflects the representation capacity of the neural network, while the proportion of consistently classified perturbed samples empirically reflects the anti-perturbation ability.

Normally, the anti-perturbation ability can be estimated by the following formula

$$\|f(x) - f(x')\|_\infty \leq L\|x - x'\|_\infty, \quad (\text{III.3})$$

where L is the Lipschitz constant, the smaller its value, the higher the anti-perturbation ability of the network.

Remark 1. *The robustness of a network is actually determined by both its representation capacity (III.1) and anti-perturbation ability (III.2). Larger neural networks usually possess better representation capacity, which in turn raises the upper limit of robustness. However, as pointed out by recent studies [14], [36], large neural networks may suffer from a degradation in perturbation resistance due to potentially large Lipschitz constants.*

In the following section, we mainly focus on the anti-perturbation ability of the network from the perspective of the convolutional feature maps.

B. The relationship between convolutional features and perturbation resistance

A common deep convolutional network $f(\cdot)$ for classification can be depicted as

$$f(\cdot) = h \circ \mathcal{P} \circ g(\cdot), \quad (\text{III.4})$$

where h denotes the classifier, \mathcal{P} is the pooling operator, and $g(\cdot)$ is the convolutional part that maps the input to the corresponding feature representation.

Note that the classifier h determines the category of an input through its convolutional and pooled feature representation, so the nature of $\mathcal{P} \circ g(\cdot)$ is critical to the robustness of network. For a given sample x and a perturbation δ , the absolute difference $|\mathcal{P}(g(x + \delta)) - \mathcal{P}(g(x))|$ reflects the disturbed magnitude of the feature, the smaller it is, the better the anti-perturbation ability of the network. Next, we will study the property of the difference $|\mathcal{P}(g(x + \delta)) - \mathcal{P}(g(x))|$ in detail.

For an input perturbation δ , let γ denote the disturbed magnitude of the output. The following inequality measures the perturbation resistance of $\mathcal{P} \circ g(\cdot)$ from a probabilistic perspective.

$$\mathbb{P}(|\mathcal{P}(g(x + \delta)) - \mathcal{P}(g(x))| \geq \gamma) \leq p, \quad (\text{III.5})$$

where $0 \leq p \leq 1$ denotes a probability. For a given p and a perturbation δ from certain distribution, the smaller γ is, the better the perturbation resistance is.

Next, under some assumptions, we derive two sufficient conditions for (III.5) to hold, one based on average pooling and the other based on max pooling. Then from these two conditions, we can discover key convolutional configurations related to perturbation resistance.

Without loss of generality, we assume that $g(\cdot) \in \mathbb{R}^{C \times H \times W}$, where C denotes the number of channels. For the convenience of discussion, we set $C = 1$ in the proof.

Proposition 1. For any sample x , let $g(x) \in \mathbb{R}^{H \times W}$ denote the corresponding convolutional feature. Assume that the input perturbation δ follows a probability distribution D such that the elements of $d(\delta) = g(x + \delta) - g(x)$ are independent from each other and $\mathbb{E}_\delta(d_{ij}(\delta)) = 0$ for all $1 \leq i \leq H, 1 \leq j \leq W$. Let

$$a = \min_{\substack{i,j \\ \delta \sim \mathcal{D}}} d_{ij}(\delta), \quad b = \max_{\substack{i,j \\ \delta \sim \mathcal{D}}} d_{ij}(\delta).$$

Then (III.5) holds true when \mathcal{P} is average pooling and

$$2 \exp \left(- \frac{2HW\gamma^2}{(b-a)^2} \right) \leq p, \quad (\text{III.6})$$

or when \mathcal{P} is max pooling and

$$\frac{(b-a)\sqrt{\log \sqrt{2HW}}}{\gamma} \leq p. \quad (\text{III.7})$$

Proof. First, notice that $\mathcal{P}(d) = \frac{1}{HW} \sum_{i,j=1}^{H,W} d_{i,j}$ if the average pooling is applied. Applying the Hoeffding's inequality [1] on the interval $[\frac{a}{HW}, \frac{b}{HW}]$, we have

$$\mathbb{P}(|\mathcal{P}(d)| \geq \gamma) \leq 2 \exp \left(- \frac{2HW\gamma^2}{(b-a)^2} \right).$$

Therefore, (III.5) holds if

$$2 \exp \left(- \frac{2HW\gamma^2}{(b-a)^2} \right) \leq p,$$

which comes to our first conclusion (III.6).

Secondly, note that $\mathcal{P}(d) = \max_{1 \leq i \leq H, 1 \leq j \leq W} d_{i,j}$ if the max pooling is applied. Define the following logarithmic moment-generating function $\psi_{d_{ij}}(\lambda) = \log \mathbb{E}_\delta e^{\lambda d_{ij}}$, where λ is a variable to be determined later. Using the Hoeffding's lemma [1] yields

$$\psi_{d_{ij}}(\lambda) \leq \frac{\lambda^2(b-a)^2}{8}, \quad \forall i, j. \quad (\text{III.8})$$

Then, it follows from the Jensen's inequality [27] and (III.8) that

$$\begin{aligned} & \exp(\lambda \mathbb{E}_\delta \max_{i,j} |d_{i,j}|) \\ & \leq \mathbb{E}_\delta \exp(\lambda \max_{i,j} |d_{i,j}|) \\ & \leq \sum_{i,j=1}^{H,W} (\mathbb{E}_\delta \exp(\lambda d_{ij}) + \mathbb{E}_\delta \exp(-\lambda d_{ij})) \\ & \leq 2HW \exp(\lambda^2(b-a)^2/8). \end{aligned}$$

Taking logarithm on both sides yields

$$\mathbb{E}_\delta \max_{i,j} |d_{ij}| \leq \frac{\log 2HW}{\lambda} + \frac{\lambda(b-a)^2}{8}.$$

Setting $\lambda = \sqrt{8 \log 2HW / (b-a)^2}$ gives

$$\mathbb{E}_\delta \max_{i,j} |d_{ij}| \leq \sqrt{\frac{(b-a)^2 \log 2HW}{2}}.$$

Using the Markov's inequality [1] and the above estimation, we have

$$\begin{aligned} \mathbb{P}(|\mathcal{P}(d)| \geq \gamma) & \leq \mathbb{P}(\max_{i,j} |d_{ij}| \geq \gamma) \\ & \leq \frac{\mathbb{E}_\delta \max_{i,j} |d_{ij}|}{\gamma} \\ & \leq \frac{(b-a)\sqrt{\log \sqrt{2HW}}}{\gamma}. \end{aligned}$$

Therefore, (III.5) holds if

$$\frac{(b-a)\sqrt{\log \sqrt{2HW}}}{\gamma} \leq p,$$

which comes to our second conclusion (III.7). \square

According to Proposition 1, we can find that given an input perturbation δ and a probability p , for average pooling,

when the feature size HW becomes larger, a smaller γ , corresponding to a better anti-perturbation ability, can ensure (III.5) holds. On the contrary, it can be inferred from (III.7) that for max pooling, a smaller γ requires a smaller feature size. Nevertheless, a small feature size usually corresponds to a low representation capacity [2]. Therefore, such trade-off makes it difficult to determine an appropriate feature size before max pooling for robustness improvement. In a conclusion, the theoretical results in Proposition 1 suggest that enlarging convolutional features before average pooling is a favorable way to enhance robustness.

Now we use a toy example to empirically verify our findings. A randomly initialized CNN, which has 4 convolutional layers (with 3, 16, 32 and 64 channels, respectively) followed by average pooling or max pooling, are considered. After uniformly sampling 1000 input perturbations in $[-0.1, 0.1]$, we plot the corresponding output disturbances at different feature scales. Although some assumptions in Proposition 1 can not be strictly satisfied, the observed phenomenon in Figure 2 is still consistent with our analysis. The disturbance after average pooling is small, and becomes further smaller as the feature size increases. On the contrary, once max pooling is applied, the output disturbance gets larger with the increase of feature size. The reader can refer to Appendix A for more experimental results.

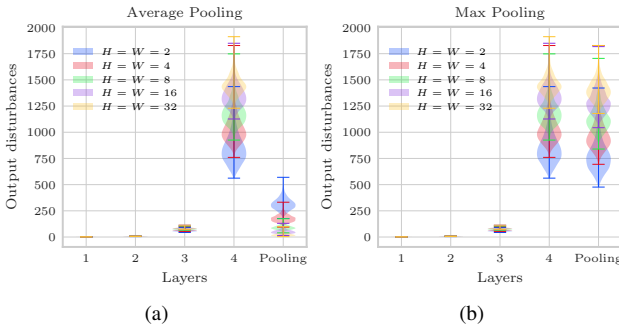


Fig. 2. The ℓ_∞ disturbances of the output features on different layers, with the input perturbation satisfying $\delta \sim \mathcal{U}[-0.1, 0.1]$. (a) A randomly initialized CNN followed by average pooling; (b) A randomly initialized CNN followed by max pooling.

Remark 2. Two assumptions on $g(x + \delta) - g(x)$ have been adopted in Proposition 1. One is the zero-mean assumption. This assumption holds in some cases, such as when $g(\cdot)$ is linear. The second is about the independence between the feature dimensions. This is a strict requirement not easy to meet in practice. However, our experiments show that the proposed method is still effective even if the network does not satisfy these assumptions.

Remark 3. It is worth mentioning that a larger feature size before average pooling does not necessarily guarantee better perturbation resistance, because the term $(b - a)$ is also positively related to HW . Too large feature size may lead to a smaller $\frac{HW}{(b - a)^2}$, which results in a bigger γ . Fortunately, we find from experiments that in many cases $\frac{HW}{(b - a)^2}$ will get

larger as HW becomes larger.

IV. TWO FEASIBLE WAYS TO ENHANCE ROBUSTNESS

According to the analysis in the previous section, expanding the convolutional feature size before average pooling could be helpful for robustness enhancement. If the original network adopts max pooling, we may modify it for better robustness by using average pooling instead.

A. Upsampling inputs

A straightforward way to enlarge output feature dimensions of a layer is upsampling the corresponding input. For example, classical interpolators such as bilinear or nearest interpolation can be applied to upscale the input (see Figure 3a for an illustration of using nearest interpolation), then the subsequent output features will also be scaled up proportionally.

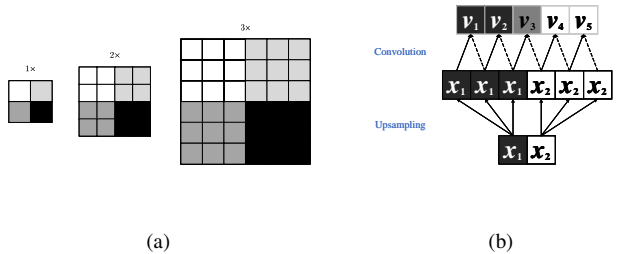


Fig. 3. (a) Upsampling the input using nearest interpolation with different scales. (b) An illustration of feature redundancy caused by unsampling.

However, this method may yield redundant feature dimensions. Let us demonstrate such problem using a one-dimensional example. As shown in Figure 3b, for an input $x \in \mathbb{R}^2$, when we enlarge it by 3 times using nearest interpolation and then apply a 2-dimensional filter, we obtain an output feature vector $v = (v_1, v_2, \dots, v_5)$. However, no matter what value the filter takes, $v_1 = v_2$ and $v_4 = v_5$ always hold true. This means that although the output feature appears to be 5-dimensional, it is actually only 3-dimensional and therefore less representative. The experimental results in the V-B section will further reflect this problem.

In order to remedy the above problem, we will put forward a more effective method in the next subsection.

B. Shrinking sliding strides

Let us take a closer look at the convolution operation. Convolving the filter $w \in \mathbb{R}^{k \times k}$ across an input $X \in \mathbb{R}^{H \times W}$ in a cross-correlation manner [10] can be expressed as

$$[X \star w]_{ij} = \sum_{m=1}^k \sum_{n=1}^k w_{mn} X_{i+m-1, j+n-1}. \quad (\text{IV.1})$$

In order to reduce the computational cost, the actual convolution used will skip some of positions. For example, sampling

every s positions in each direction gives the following down-sampled convolution operation

$$[X \star w]_{ij} = \sum_{m=1}^k \sum_{n=1}^k w_{mn} X_{(i-1)s+m, (j-1)s+n}, \quad (\text{IV.2})$$

where s is called the *sliding stride*. Now the corresponding output feature dimensions H and W are determined by

$$\begin{aligned} H &= \lfloor \frac{\mathfrak{H} + 2p - k}{s} + 1 \rfloor, \\ W &= \lfloor \frac{\mathfrak{W} + 2p - k}{s} + 1 \rfloor, \end{aligned} \quad (\text{IV.3})$$

where p is the padding that allows the input to be downsampled exactly to $1/s$.

It is evident from (IV.3) that shrinking the stride s can make the output convolutional feature become larger, producing a similar effect as upsampling the input, but without the previous feature redundancy problem.

Now we take common ResNet as an example to illustrate how to modify the stride configurations. As shown in Figure 4, the convolutional part of a typical ResNet consists of 4 intermediate stages, each of which contains several convolutional layers. We only need to modify the stride of the first convolutional layer at each stage. Denote by the original sliding stride configuration as $s_1-s_2-s_3-s_4$ (1-2-2-2 in common ResNet). If we modify it to $s_1-\frac{s_2}{2}-s_3-s_4$, then all convolutional features after the second stage will be upscaled by a factor of 2, resulting in a final enlarged feature before pooling.

Remark 4. Of course, the 1-1-2-2 and 1-2-1-2 stride configurations can lead to the same feature size for pooling. But the configuration 1-2-2-2 is still preferred as it contributes to better representation capacity.

For modifications on other neural network architectures such as AlexNet and VGG16, the reader can refer to Appendix B.

V. EXPERIMENTS

A. Experimental setup

TABLE I
THE BASIC SETUP FOR ADVERSARIAL ATTACKS IN ℓ_∞ NORM.

| | FGSM | PGD | PGD | PGD | DeepFool | AutoAttack |
|----------------------|------|------|------|----------|----------|------------|
| number of iterations | - | 10 | 20 | 50 | 50 | - |
| step size | - | 0.25 | 0.25 | 0.033333 | 0.02 | - |

Baseline defenses. We implement the baselines including AT [20], ALP [16], TRADES [38], MART [33], FAT [39] and AWP [35], identically following the settings suggested in original papers. All adversarial samples required in the procedure of training are crafted on the fly by PGD-10 within $\epsilon = 8/255$. In particular, we apply an early-stopping learning schedule [23] to AT, ALP and TRADES, namely, the SGD optimizer with an initialized learning rate of 0.1 which is decayed by a factor 10 at 100 and 105 epoch.

Attacks. To reliably evaluate adversarial robustness of defense methods, several benchmark attacks including FGSM

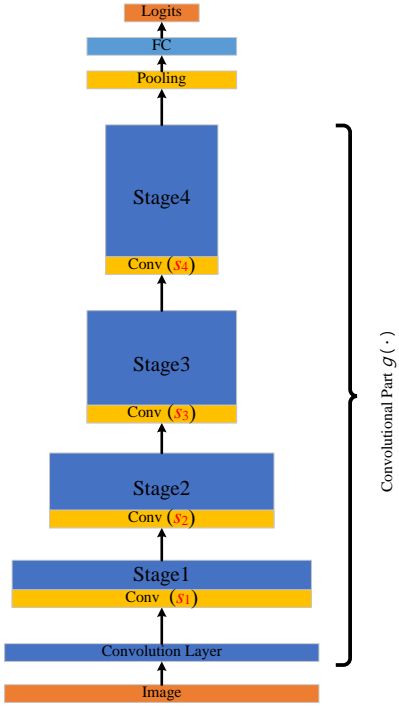


Fig. 4. The architecture of ResNet, whose convolutional part includes 4 intermediate stages. The stride of the first convolutional layer at each stage is denoted as s_i , $i = 1, 2, \dots, 4$, which can be scaled down to produce larger convolutional features for pooling.

[9], PGD [20], DeepFool [21] and AutoAttack [5] are employed. All implementations are provided by FoolBox [24] except AutoAttack from the source code of [5]. The major settings of these attacks are listed in Table I, wherein step size denotes the relative step size of PGD and the overshoot of DeepFool, respectively.

Architectures. Besides the widely used ResNet18 [12], we also try to explore proper stride configurations for other networks including AlexNet [18], VGG16 [30] and PreActResNet18 [13] (see Appendix B for architecture details of AlexNet and VGG16). In what follows, we use e.g. $s_1-s_2-s_3-s_4$ to denote specific stride configurations.

B. Upsampling inputs versus shrinking sliding strides

We first compare the two proposed methods from three aspects: representation capacity, anti-perturbation ability and computational efficiency.

Both standard training and adversarial training will be conducted on CIFAR-10 using ResNet18. TRADES [38] is adopted as the representative of adversarial training because it rarely kills the training in the first iterations. In addition, unless otherwise stated, the robustness reported in the following are empirically evaluated by PGD-20.

Representation capacity. In Section III-B we have pointed out that enlarging convolutional feature size is helpful to promote the representation capacity of the network. We are to verify this point first, and use the classification accuracy on clean data to measure the representation capacity of the network.

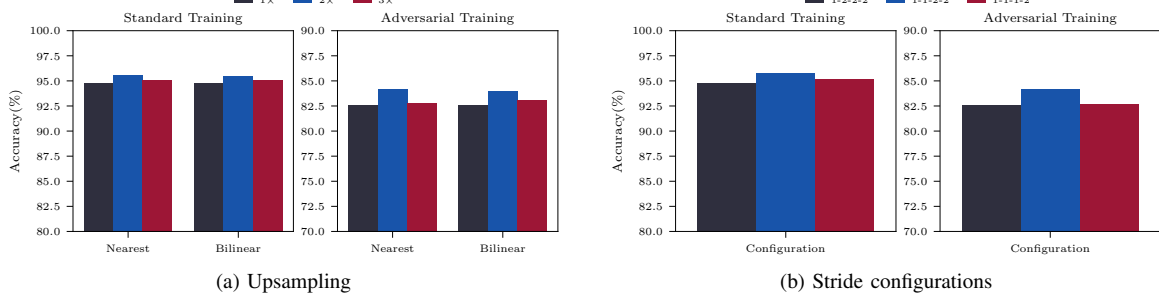


Fig. 5. Natural accuracy (%) comparisons of ResNet18 and its modified versions on CIFAR-10. (a) Upsampling using bilinear or nearest interpolation under different scales; (b) Shrinking sliding strides using various configurations.

We can see from Figure 5 that the two methods show similar performance here, and the classification accuracy of the modified network always outperforms that of the baseline, regardless by standard training or adversarial training.

It is worth to note that the classification accuracy is not consistently better with larger features. When the magnification factor is greater than 2 (red), the corresponding classification accuracy decreases. There may be two reasons for this phenomenon. First, neurons become redundant when the magnification factor is large enough. Second, excessive shrinkage of sliding stride slows down the growth of receptive field, and in turn deteriorates the learning ability of the network. As can be seen from Figure 6, the modified ResNet18 configured as 1-1-1-2 can not get global information until the 16-th layer.

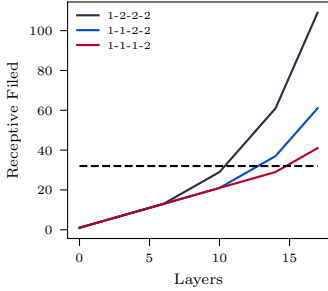


Fig. 6. Receptive field of ResNet18 with various stride configurations. The horizontal dotted line therein indicates the image size 32.

Anti-perturbation ability. We use the proportion of samples, whose classification results remain unchanged after perturbation, to measure the anti-perturbation ability of the network. Here we only care about the invariance of the predicted results, regardless of the correctness.

Table II provides the performance of various modified ResNet versions, where the best results are achieved in 2 \times and 1-1-2-2 configurations, both corresponding to upscaling the convolutional feature size by a factor of 2. And since 1-1-2-2 and 1-1-1-2 have a similar perturbation resistance performance, in view of the adversarial training results in Figure 5b, we can infer that such gain is due to the enhanced perturbation resistance rather than representation capacity.

Furthermore, we find that under higher perturbation budgets, when the amplification factor is enlarged from 2 to 3,

TABLE II
THE PROPORTION (%) OF UNCHANGED PREDICTED RESULTS ON
CIFAR-10 UNDER VARIOUS PERTURBATION BUDGETS ϵ . **TOP:**
UPSAMPLE USING NEAREST OR BILINEAR INTERPOLATION; **BOTTOM:**
DIFFERENT SLIDING STRIDE CONFIGURATIONS.

| | ϵ, ℓ_∞ | | | | | |
|------------------------|-------------------------|--------------|--------------|--------------|--------------|--------------|
| | 0 | 2/255 | 4/255 | 6/255 | 8/255 | 10/255 |
| ResNet18 (1 \times) | 100 | 86.54 | 75.66 | 65.48 | 55.67 | 45.91 |
| Nearest (2 \times) | 100 | 87.59 | 76.97 | 66.72 | 57.11 | 47.30 |
| Nearest (3 \times) | 100 | 87.17 | 75.62 | 65.60 | 55.71 | 46.82 |
| Bilinear (3 \times) | 100 | 86.74 | 76.29 | 65.81 | 55.99 | 46.53 |
| 2-2-2-2 | 100 | 85.05 | 73.19 | 61.80 | 51.61 | 42.31 |
| ResNet18 (1-2-2-2) | 100 | 86.54 | 75.66 | 65.48 | 55.67 | 45.91 |
| 1-1-2-2 | 100 | 87.78 | 76.86 | 66.39 | 57.11 | 47.44 |
| 1-1-1-2 | 100 | 86.92 | 76.16 | 65.82 | 56.59 | 47.26 |

the resistance performance of upsampling approach decreases significantly, whereas the method of shrinking strides does not have such a phenomenon. This just reflects what was discussed in Section IV-A that interpolation-based upsampling may lead to feature redundancy and thus weaken the learning ability of the model.

Computational efficiency. Figure 7 compares the floating point operations (Flops) and the total memory required for the two strategies. Because the modified stride configuration is still applied to the original image, it requires much less memory and computational cost. On the contrary, upsampling inputs consumes more theoretical Flops on meaningless redundant elements. Notably, this computational gap will widen further in practice, especially in the procedure of adversarial training.

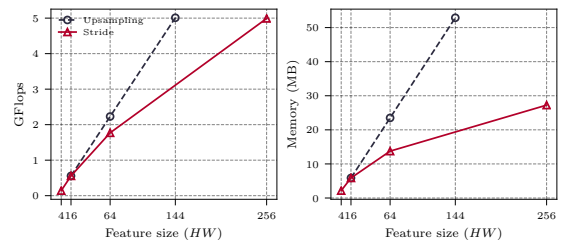


Fig. 7. Computational costs of the inference on a 32×32 image. **Left:** Floating point operations (Flops); **Right:** Total memory.

According to the above three groups of experiments, we can conclude that 1) properly enlarging features are capable of improving the representation capacity and anti-perturbation

ability; 2) stride shrinking is more effective in improving anti-perturbation ability than upsampling the inputs.

C. Average pooling versus Max pooling

In this subsection, we will adopt the stride shrinking method for ResNet18 on CIFAR-10, and empirically demonstrate the role of average pooling and max pooling.

As shown in Table III, under the original configuration (1-2-2-2), average pooling or max pooling make little difference on both natural accuracy and adversarial robustness. But, once the convolutional feature size is enlarged (1-1-2-2), average pooling can improve the natural accuracy and adversarial robustness by 2.99% and 2.5%, respectively, whereas max pooling leads to worse performance. This is exactly what Proposition 1 suggests that enlarging feature size before average pooling, but not before max pooling, is essential for robustness enhancement.

TABLE III

NATURAL ACCURACY (%) AND ROBUSTNESS (%) UNDER PGD-20 ON CIFAR-10 USING AVERAGE POOLING AND MAX POOLING, RESPECTIVELY. THE UNDERLINE INDICATES THE MODIFIED CONFIGURATION.

| | Pooling Type | Natural | PGD-20 |
|---------|--------------|---------|--------|
| 1-2-2-2 | Average | 82.56 | 53.50 |
| | Max | 81.49 | 53.29 |
| 1-1-2-2 | Average | 84.13 | 55.37 |
| | Max | 81.12 | 52.87 |

D. Improvement on various neural network architectures

TABLE IV

NATURAL ACCURACY (%) AND ROBUSTNESS (%) UNDER PGD-20 ATTACK OF VARIOUS NEURAL NETWORK ARCHITECTURES ON CIFAR-10. THE UNDERLINE INDICATES THE MODIFIED CONFIGURATION.

| | Configuration | Natural | PGD-20 |
|----------------|------------------|--------------|--------------|
| AlexNet | 2-2-2-2 | 70.56 | 36.57 |
| | <u>1-1-2-2</u> | 76.29 | 39.50 |
| VGG16 | 2-2-2-2-2 | 79.61 | 43.28 |
| | <u>1-1-2-2-2</u> | 84.47 | 48.61 |
| ResNet18 | 1-2-2-2 | 82.56 | 53.50 |
| | <u>1-1-2-2</u> | 84.13 | 55.37 |
| PreActResNet18 | 1-2-2-2 | 82.58 | 53.05 |
| | <u>1-1-2-2</u> | 83.92 | 54.64 |

Table IV shows that properly modifying the stride configuration can indeed help the performance of various network architectures. Note that even though AlexNet and VGG16 have a long chain of fully connected layers after the convolutional part, they still enjoy consistent accuracy and robustness gains from the modified configuration. In addition, the performance gains of AlexNet and VGG16 far exceed those of ResNet18, which is mainly because their original configuration contains more unsatisfactory downsampling operations, so after shrinking the sliding strides, bigger gains can be achieved.

E. Extensive robustness evaluation

Our approach is orthogonal to most of existing defense methods. In this section, we take RestNet18 as the baseline neural network architecture, and demonstrate the power of our approach using various defensive models on the CIFAR-10 and CIFAR-100 datasets.

As shown in Tables V and VI, desirable robustness gains of 1% ~ 2% can be consistently achieved, from the simplest FGSM attack to the most aggressive AutoAttack. In particular, the TRADES with 1-1-2-2 stride configuration even performs comparable to the current state-of-the-art adversarial training model AWP. Furthermore, it is observed that our approach can also ensure a consistent improvement on natural accuracy, and there is no unsatisfactory trade-off between natural accuracy and robustness as in most of the previous literature.

Although there is no improvement when using the standard FAT model on CIFAR-10, mainly due to overfitting, an improvement could still be achieved after applying the earlier stoppage strategy [25]. Especially, non-trivial gains are observed on the best checkpoint evaluated by PGD-10.

VI. CONCLUSION

In this work, we theoretically analyze the relationship between the convolutional features and perturbation resistance of the network. It is discovered that enlarging the convolutional feature size before average pooling is capable of reconciling both natural accuracy and adversarial robustness. Based on the theoretical findings, we propose two methods to modify the convolutional layer configurations, which greatly enhance the robust performance of existing network architectures. Our research helps expand the understanding of network robustness and brings new inspiration to the design of robust deep learning models.

We leave a number of issues for future research: 1) Some of the assumptions in Proposition 1 are strict, and a relaxed version will be preferred. 2) How to quantitatively decide an optimal stride configuration is an interesting problem that needs further research. From our understanding, the receptive field should be taken into account.

REFERENCES

- [1] Boucheron S., Lugosi G. & Massart P. Concentration inequalities: A nonasymptotic theory of independence. *Oxford university press*, 2013.
- [2] Cao Y. & Gu Q. Generalization bounds of stochastic gradient descent for wide and deep neural networks. In *Advances in Neural Information Processing Systems (NIPS)*, 2019.
- [3] Carlini N. & Wagner D. Towards evaluating the robustness of neural networks. In *IEEE Symposium on Security and Privacy (SP)*, 2017.
- [4] Cohen J., Rosenfeld E. & Kolter J. Certified adversarial robustness via randomized smoothing. In *International Conference on Machine Learning (ICML)*, 2019.
- [5] Croce F. & Hein Matthias. Reliable evaluation of adversarial robustness with an ensemble of diverse parameter-free attacks. In *International Conference on Machine Learning (ICML)*, 2020.
- [6] Dai S., Mahloujifar S. & Mittal P. Parameterizing activation functions for adversarial robustness. *arXiv preprint arXiv:2110.05626*, 2021.
- [7] Dosovitskiy A., Beyer L., Kolesnikov A., Weissenborn D., Zhai X., Unterthiner T., Dehghani M., Minderer M., Heigold G., Gelly S., Uszkoreit J. & Houlsby N. An image is worth 16x16 words: transformers for image recognition at scale. In *International Conference on Learning Representations (ICLR)*, 2021.

TABLE V

NATURAL ACCURACY (%) AND ROBUSTNESS (%) UNDER VARIOUS ATTACKS WITHIN THE PERTURBATION BUDGET $\epsilon = 8/255$ ON CIFAR-10. \dagger : APPLYING THE LEARNING SCHEDULE [23] FOR EARLY STOPPING; \ddagger : THE BEST RESULT ON THE CHECKPOINT EVALUATED BY PGD-10. UNDERLINE INDICATES THE MODIFIED RESNET18.

| | Natural | | FGSM | | PGD-20 | | PGD-50 | | DeepFool | | AutoAttack | |
|-----------------------|---------|------------------|---------|--------------------|---------|--------------------|---------|--------------------|----------|--------------------|------------|--------------------|
| | 1-2-2-2 | 1-1-2-2 | 1-2-2-2 | <u>1-1-2-2</u> | 1-2-2-2 | <u>1-1-2-2</u> | 1-2-2-2 | <u>1-1-2-2</u> | 1-2-2-2 | <u>1-1-2-2</u> | 1-2-2-2 | <u>1-1-2-2</u> |
| AT \dagger [20] | 84.15 | 86.17 \uparrow | 58.85 | 60.70 \uparrow | 52.80 | 53.24 \uparrow | 52.50 | 53.18 \uparrow | 54.32 | 55.90 \uparrow | 48.72 | 49.83 \uparrow |
| ALP \dagger [16] | 86.53 | 88.11 \uparrow | 58.73 | 59.21 \uparrow | 50.88 | 51.36 \uparrow | 50.76 | 51.27 \uparrow | 54.47 | 55.39 \uparrow | 47.38 | 49.00 \uparrow |
| TRADES \dagger [38] | 82.56 | 84.13 \uparrow | 58.06 | 59.60 \uparrow | 53.50 | 55.37 \uparrow | 53.37 | 55.28 \uparrow | 54.50 | 56.05 \uparrow | 49.71 | 51.24 \uparrow |
| MART [33] | 82.77 | 84.67 \uparrow | 59.28 | 60.46 \uparrow | 52.44 | 53.00 \uparrow | 52.28 | 52.91 \uparrow | 54.07 | 54.58 \uparrow | 47.29 | 47.97 \uparrow |
| MART \ddagger [33] | 79.23 | 79.47 \uparrow | 58.44 | 59.23 \uparrow | 54.93 | 55.93 \uparrow | 54.94 | 55.85 \uparrow | 52.20 | 52.66 \uparrow | 47.83 | 48.59 \uparrow |
| FAT [39] | 87.34 | 88.31 \uparrow | 55.28 | 53.43 \downarrow | 43.90 | 42.55 \downarrow | 43.79 | 42.39 \downarrow | 51.20 | 50.04 \downarrow | 41.56 | 40.93 \downarrow |
| FAT \ddagger [39] | 87.55 | 88.86 \uparrow | 56.38 | 57.42 \uparrow | 46.67 | 46.91 \uparrow | 46.56 | 46.83 \uparrow | 52.54 | 53.39 \uparrow | 44.10 | 44.95 \uparrow |
| AT-AWP [35] | 82.32 | 84.05 \uparrow | 59.47 | 60.41 \uparrow | 54.47 | 54.75 \uparrow | 54.40 | 54.59 \uparrow | 54.63 | 55.30 \uparrow | 49.52 | 50.23 \uparrow |
| TRADES-AWP [35] | 82.69 | 84.36 \uparrow | 59.96 | 61.39 \uparrow | 55.90 | 57.14 \uparrow | 55.88 | 57.10 \uparrow | 55.94 | 57.65 \uparrow | 51.84 | 53.51 \uparrow |

TABLE VI

NATURAL ACCURACY (%) AND ROBUSTNESS (%) UNDER VARIOUS ATTACKS WITHIN THE PERTURBATION BUDGET $\epsilon = 8/255$ ON CIFAR-100. \dagger : APPLYING THE LEARNING SCHEDULE [23] FOR EARLY STOPPING; \ddagger : THE BEST RESULT ON THE CHECKPOINT EVALUATED BY PGD-10. UNDERLINE INDICATES THE MODIFIED RESNET18.

| | Natural | | FGSM | | PGD-20 | | PGD-50 | | DeepFool | | AutoAttack | |
|-----------------------|---------|------------------|---------|------------------|---------|------------------|---------|------------------|----------|--------------------|------------|--------------------|
| | 1-2-2-2 | 1-1-2-2 | 1-2-2-2 | <u>1-1-2-2</u> | 1-2-2-2 | <u>1-1-2-2</u> | 1-2-2-2 | <u>1-1-2-2</u> | 1-2-2-2 | <u>1-1-2-2</u> | 1-2-2-2 | <u>1-1-2-2</u> |
| AT \dagger [20] | 59.16 | 62.50 \uparrow | 32.95 | 35.30 \uparrow | 28.88 | 31.15 \uparrow | 28.87 | 31.05 \uparrow | 28.32 | 30.24 \uparrow | 25.16 | 27.04 \uparrow |
| ALP \dagger [16] | 63.41 | 66.70 \uparrow | 30.45 | 32.05 \uparrow | 25.33 | 26.81 \uparrow | 25.34 | 26.70 \uparrow | 26.51 | 27.65 \uparrow | 23.13 | 24.06 \uparrow |
| TRADES \dagger [38] | 58.69 | 59.05 \uparrow | 32.59 | 33.66 \uparrow | 30.22 | 31.27 \uparrow | 30.17 | 31.21 \uparrow | 28.06 | 27.97 \downarrow | 25.37 | 25.73 \uparrow |
| MART [33] | 54.74 | 56.01 \uparrow | 34.05 | 35.02 \uparrow | 31.67 | 32.90 \uparrow | 31.70 | 32.87 \uparrow | 28.42 | 29.04 \uparrow | 26.24 | 26.59 \uparrow |
| MART \ddagger [33] | 54.05 | 55.00 \uparrow | 34.43 | 35.52 \uparrow | 32.31 | 33.75 \uparrow | 32.29 | 33.76 \uparrow | 28.58 | 29.12 \uparrow | 26.47 | 27.12 \uparrow |
| FAT [39] | 62.23 | 64.72 \uparrow | 26.75 | 26.86 \uparrow | 20.01 | 20.20 \uparrow | 20.04 | 20.11 \uparrow | 23.29 | 23.42 \uparrow | 18.89 | 18.65 \downarrow |
| FAT \ddagger [39] | 63.69 | 66.40 \uparrow | 28.19 | 29.17 \uparrow | 22.01 | 22.68 \uparrow | 21.90 | 22.69 \uparrow | 24.48 | 25.17 \uparrow | 20.05 | 20.82 \uparrow |
| AT-AWP [35] | 58.47 | 61.37 \uparrow | 35.37 | 37.22 \uparrow | 32.65 | 34.23 \uparrow | 32.60 | 34.13 \uparrow | 30.12 | 31.65 \uparrow | 27.47 | 28.64 \uparrow |
| TRADES-AWP [35] | 59.53 | 60.81 \uparrow | 34.23 | 35.22 \uparrow | 31.96 | 32.59 \uparrow | 31.87 | 32.50 \uparrow | 29.34 | 29.55 \uparrow | 26.57 | 26.94 \uparrow |

[8] Glorot X & Bengio Y. Understanding the difficulty of training deep feedforward neural networks. In *International Conference on Artificial Intelligence and Statistics (AISTATS)*, 2010.

[9] Goodfellow I. J., Shlens J. & Szegedy C. Explaining and harnessing adversarial examples. In *International Conference on Learning Representations (ICLR)*, 2015.

[10] Goodfellow I. J., Bengio Y. & Courville A. Deep learning. *MIT press*, 2016.

[11] Gowal S., Qin C., Uesato J., Mann T. & Kohli, P. Uncovering the limits of adversarial training against norm-bounded adversarial examples. *arXiv preprint arXiv:2010.03593*, 2020.

[12] He K., Zhang X., Ren S. & Sun J. Deep residual learning for image recognition. In *IEEE Conference on Computer Vision and Pattern Recognition (CVPR)*, 2016.

[13] He K., Zhang X., Ren S. & Sun J. Identity mappings in deep residual networks. *arXiv preprint arXiv:1603.05027*, 2016.

[14] Huang H., Wang Y., Erfani S., Gu Q., Bailey J. & Ma X. Exploring architectural ingredients of adversarially robust deep neural networks. In *Advances in Neural Information Processing Systems (NIPS)*, 2021.

[15] Ilyas A., Santurkar S., Tsipras D., Engstrom L., Tran B. & Madry A. Adversarial examples are not bugs, they are features. In *Advances in Neural Information Processing Systems (NIPS)*, 2019.

[16] Kannan H., Kurakin A. & Goodfellow I. J. Adversarial logit pairing. *arXiv preprint arXiv:1803.06373*, 2018.

[17] Krizhevsky A. & Hinton G. E. Learning multiple layers of features from tiny images. *Technical report, Citeseer*, 2009.

[18] Krizhevsky A., Sutskever I. & Hinton G. E. ImageNet classification with deep convolutional neural networks. In *Advances in Neural Information Processing Systems (NIPS)*, 2012.

[19] LeCun Y., Chopra S., Hadsell R., Ranzato M. & Huang F. A tutorial on energy-based learning. In *Predicting Structured Data*, *MIT Press*, 2006.

[20] Madry A., Makelov A., Schmidt L. & Tsipras D. Towards deep learning models resistant to adversarial attacks. In *International Conference on Learning Representations (ICLR)*, 2018.

[21] Moosavi-Dezfooli S., Fawzi A. & Frossard P. DeepFool: a simple and accurate method to fool deep neural networks. In *IEEE Conference on Computer Vision and Pattern Recognition (CVPR)*, 2016.

[22] Pang T., Xu K., Dong Y., Du C., Chen N. & Zhu J. Rethinking softmax cross-entropy loss for adversarial robustness. In *International Conference On Learning Representations (ICLR)*, 2020.

[23] Pang T., Yang X., Dong Y., Su H. & Zhu J. Bag of tricks for adversarial training. In *International Conference on Learning Representations (ICLR)*, 2020.

[24] Rauber J., Brendel W. & Bethge M. Foolbox v0.8.0: A Python toolbox to benchmark the robustness of machine learning models. *arXiv preprint arXiv:1707.04131*, 2017

[25] Rice L., Wong E. & Kolter J. Z. Overfitting in adversarially robust deep learning. In *International Conference on Machine Learning (ICML)*, 2020.

[26] Rebuffi S., Gowal S., Calian D. A., Stimberg F., Wiles O. & Mann T. Fixing data augmentation to improve adversarial robustness. *arXiv preprint arXiv:2103.01946*, 2021.

[27] Rudin W. Real and complex analysis. *McGraw-Hill*, 1978.

[28] Salman H., Li J., Razenshteyn I. P., Zhang P., Zhang H., Bubeck S. & Yang, G. Provably robust deep learning via adversarially trained smoothed classifiers. In *Advances in Neural Information Processing Systems (NIPS)*, 2019.

[29] Shao R., Shi Z., Yi J., Chen P. & Hsieh C. On the adversarial robustness of vision transformers. *arXiv preprint arXiv:2103.15607*, 2021.

[30] Simonyan K. & Zisserman A. Very deep convolutional networks for large-scale image recognition. In *International Conference on Learning Representation (ICLR)*, 2015.

[31] Szegedy C., Zaremba W., Sutskever I., Bruna J., Erhan D. Goodfellow I. J. & Fergus R. Intriguing properties of neural networks. In *International Conference on Learning Representations (ICLR)*, 2014.

[32] Tramèr F. & Boneh D. Adversarial training and robustness for multiple perturbations. In *Advances in Neural Information Processing Systems (NIPS)*, 2019.

[33] Wang Y., Zou D., Yi J., Bailey J., Ma X. & Gu Q. Improving adversarial robustness requires revisiting misclassified examples. In *International Conference on Learning Representation (ICLR)*, 2020.

[34] Wong E., Rice L., & Kolter J. Z. Fast is better than free: Revisiting adversarial training. IN *International Conference on Learning Representations (ICLR)*, 2020.

- [35] Wu D., Xia S. & Wang Y. Adversarial weight perturbation helps robust generalization. In *Advances in Neural Information Processing Systems (NIPS)*, 2020.
- [36] Wu B., Chen J., Cai D., He X. & Gu Q. Do wider neural networks really help adversarial robustness? In *Advances in Neural Information Processing Systems (NIPS)*, 2021.
- [37] Zagoruyko S. & Komodakis N. Wide residual networks. In *British Machine Vision Conference (BMVC)*, 2016.
- [38] Zhang H., Yu Y., Jiao J., Xing E., Ghaoui L. & Jordan M. Theoretically principled trade-off between robustness and accuracy. In *International Conference on Machine Learning (ICML)*, 2019.
- [39] Zhang J., Xu X., Han B., Niu G., Cui L., Sugiyama M. & Kankanhalli M. Attacks which do not kill training make adversarial learning stronger. In *International Conference on Machine Learning (ICML)*, 2020.

APPENDIX

A. Experimental insights on Proposition 1

We further examine how the output disturbance changes under different conditions. We focus on the initial weights and the activation function. The toy neural network consists of 4 convolutional layers (3, 16, 32 and 64 channels, respectively) followed by an average pooling layer.

As shown in Figure 8, for different weight initialization methods, including Normal, Uniform, Xavier Normal and Xavier Uniform [8], the corresponding output disturbances are significantly different, which implies that the initialization of the weights has a crucial impact on the perturbation resistance of the network.

Furthermore, we find that the linear network without activation performs better, because such network is more in line with the assumptions in Proposition 1.

B. Modified Architectures of AlexNet and VGG16

We provide the architectural details of AlexNet [18] and VGG16 [30] in Figure 9, where the adaptive average pooling is performed after the convolutional part.

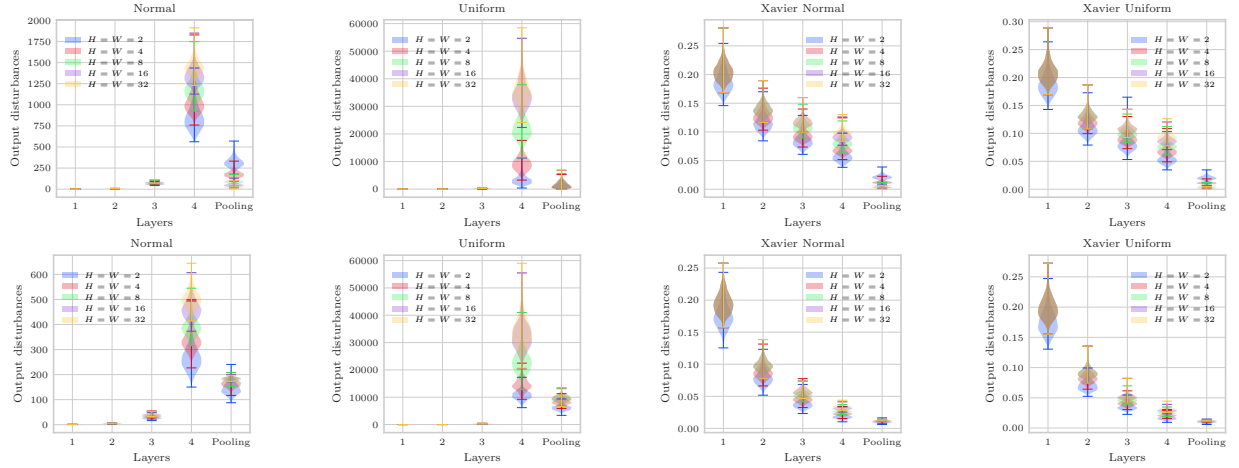


Fig. 8. The ℓ_∞ disturbances of the output features on different layers under various weight initialization strategies. The input perturbation satisfies $\delta \sim \mathcal{U}[-0.1, 0.1]$. **Top:** No activation; **Bottom:** ReLU activation.

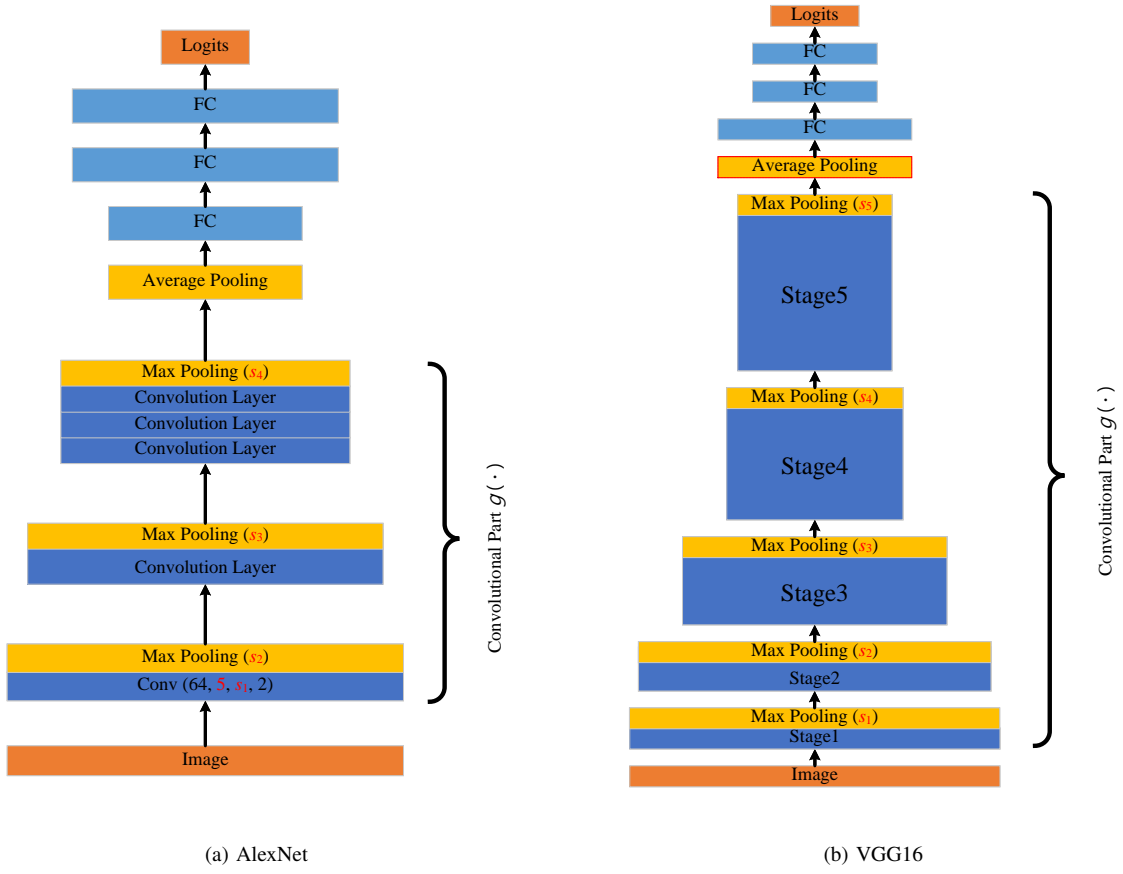


Fig. 9. The architectures of AlexNet and VGG16, where **red notations** indicate the configurations to be modified for better robustness.